JOURNAL OF CATALYSIS **167,** 198–209 (1997)
ARTICLE NO. CA971580

Partial Oxidation of Methane to Synthesis Gas Using $LnCoO_3$ Perovskites as Catalyst Precursors

R. Lago,* G. Bini,† M. A. Peña,* and J. L. G. Fierro*,[1]

*Instituto de Catálisis y Petroleoquímica, CSIC, Campus UAM, Cantoblanco, 28049 Madrid, Spain; and †Dipartimento de Chimica Industriale e Materiali, University of Bologna, Vle. Risorgimento 4, 40136 Bologna, Italy

Received August 12, 1996; revised December 12, 1996; accepted December 17, 1996

In this work a series of cobalt-containing perovskites $LnCoO_3$ (Ln = La, Pr, Nd, Sm, and Gd) has been studied as catalyst precursors for the partial oxidation of methane to synthesis gas. All the perovskite precursors were prereduced *in situ*, producing cobalt metal finely dispersed over the rare earth sesquioxide support described here as Ln–Co–O. Of the catalyst tested the system Gd–Co–O showed exceptionally better performance for CO and H_2 production (with methane conversion of 73% and selectivities of 79 and 81% for CO and H_2, respectively, at 1009 K). The production of synthesis gas over the other catalysts decreased in the following order: Sm–Co–O ≫ Nd–Co–O > Pr–Co–O. The catalyst La–Co–O was active for methane combustion and only traces of CO and H_2 were observed under the reaction conditions. XRD and XPS analyses of the catalyst La–Co–O showed that under the reaction conditions the cobalt metal is completely reoxidized, regenerating the original $LnCoO_3$ perovskite structure. For the reaction over Nd–Co–O the cobalt is only partially reoxidized to $NdCoO_3$. For Gd–Co–O and Sm–Co–O, the most stable and active catalysts for the partial oxidation of methane no reoxidation to $LnCoO_3$ was observed. TPR and XRD studies showed that the perovskite $NdCoO_3$ is reduced in two steps, first to $NdCoO_{2.5}$ and further to Co°/Nd_2O_3 and in both stages it was demonstrated that the reoxidation with O_2 is capable of recovering the perovskite structure. TPO experiments with reduced La–Co–O, Nd–Co–O, Sm–Co–O, and Gd–Co–O catalysts indicated that reoxidation of cobalt also takes place in two steps: first by oxidation of the supported Co° to the spinel Co_3O_4 ($Co^{2+}Co^{3+}{}_2O_4$) followed by a further oxidation of the Co^{2+} to Co^{3+} with a simultaneous solid state reaction with Ln_2O_3, regenerating the perovskite structure. It was observed that the temperature for the second oxidation step is strongly dependent on the nature of the lanthanide. Based on these results it is proposed that the deactivation of the catalysts Ln–Co–O by reoxidation of cobalt metal is related to the thermodynamic stability of the parent perovskite structure. We also present evidence that hydroxyl groups on the rare earth oxide, specially in the La–Co–O system, might make some contribution to the reoxidation of cobalt metal during the reaction via a reverse spillover process.

1. INTRODUCTION

The research on methane conversion has recently focused on the direct catalytic oxidation to synthesis gas:

$$CH_4 + 1/2\,O_2 \rightarrow CO + 2H_2 \quad (\Delta H^{\circ}_{298\,K} = -22.6\,\text{kJ/mol}). \qquad [1]$$

The major advantages of this route over the steam reforming are the H_2/CO ratio of ca. 2, suitable for downstream processes and the exothermicity of the reaction which eliminates the need for a fuel gas (1). Many catalysts for the partial oxidation of methane to synthesis gas, consisting of supported metals such as Ni, Co, and Fe and noble metals Pd, Ir, Rh, Ru, Pt, etc., have been described in the literature (2–9).

This work deals with the use of perovskites of the type $LnCoO_3$ as precursors of the catalyst for the partial oxidation of methane to synthesis gas. These perovskites may offer interesting features as precursors for supported metal catalysts. For example, careful reduction can be carried out in order to produce a finely dispersed transition metal over the sesquioxides Ln_2O_3. Cobalt and nickel supported on rare earth oxides have been demonstrated to be effective catalysts for methane partial oxidation. Choudhary *et al.* (10) obtained high activity and selectivity for the conversion of methane to H_2 and CO in the presence of CoO–rare earth oxide catalysts. They claimed that the reduced catalyst $CoO–Yb_2O_3$ produced methane conversion of 59.4% with 80% selectivity for H_2 and CO at temperatures as low as 673 K, far enough from the product distributions predicted by equilibrium. As already explained (5), the apparent deviation of product distributions from thermodynamic equilibrium at high space velocities may have resulted from a small hot zone in the reactor and consequently incorrect measurement of the true reaction temperature. Several papers in the recent literature report the effective role played by La_2O_3 as a support and promoter for nickel catalysts (11–14). Also, the reduction conditions of the perovskite can be varied in order to control the metal particle size which has an important effect on coke formation. It has been demonstrated that the rate of coke formation over nickel catalysts during

[1] To whom correspondence should be addressed. Fax: +34 1 585 4760. E-mail: jlgfierro@icp.csic.es.

0021-9517/97 $25.00

the steam reforming of hydrocarbon depends on the metal crystallite size. Borowiecky (15) showed that rate of coke formation increases linearly with the size of the nickel crystallites in the range from 6 to 35 nm. Rostrup-Nielsen (16) proposed that coke formation during steam reforming of methane requires a minimum of 16 neighboring sites on a nickel surface. Another way to improve the resistance to coking is to add an earth alkaline oxide such as MgO and CaO to the catalyst (17). It has been proposed that the formation of solid solution such as NiO/MgO in the catalyst precursor is responsible for the high activity and stability observed (13, 18, 19). In this respect, perovskites of the type $Ln_{1-y}A_yMO_3$ (where A is an alkaline earth and M a transition metal) is an interesting precursor to produce a finely dispersed metal containing alkaline earth oxide which might show improved coke resistance.

Hayakawa *et al.* (20) studied the perovskite $Ca_{1-x}Sr_xTiO_3$ mixed with nickel oxide for methane oxidation at 1028 K, both before and after pretreatment with methane. Before methane pretreatment the catalyst produced mainly C_2 hydrocarbons and CO_2 but no syngas. After methane pretreatment at 1048 K for 1 h, the mixture became very selective to synthesis gas, giving 70.9% conversion of methane with 94% selectivity to CO and H_2. Based on XRD analyses it was proposed that the methane pretreatment produced metallic nickel supported on the perovskite which was responsible for the synthesis gas formation. Similar results were obtained for cobalt and iron (8). Slagten and Olsbye (9) studied the systems La–M–O (M = Co, Ni, Rh, and Cr) for the partial oxidation of methane to syngas. They observed very high activity for the system La–Rh–O, whereas the catalyst La–Co–O (which was a mixture of $LaCoO_3$, La_2O_3, and Co_3O_4) produced mainly CO_2. If the catalyst La–Co–O was kept at 1073 K after 30 h reaction the activity changed to give mainly CO, which they assigned to the *in situ* reduction of cobalt.

This work presents some results on the use of cobalt containing perovskite $LnCoO_3$ as catalyst precursors for the partial oxidation of methane to synthesis gas. Different lanthanides (Ln = La, Pr, Nd, Sm, Gd, and Dy) have been used in order to study the effect of the rare earth support on the cobalt catalyst.

2. EXPERIMENTAL

All the perovskites were prepared by the method of the amorphous citrate percursor (21) and were present as pure phases with no contaminants of Ln_2O_3 or cobalt oxides according to the powder X-ray diffraction (XRD) analyses. XRD patterns were recorded with a Philips PW 1716/30 diffractometer using nickel filtered Cu$K\alpha$ radiation ($\lambda = 0.1538$ nm), under constant instrumental parameters. For each sample, Bragg's angles between 5 and 75° were scanned at a rate of 2°/min.

Temperature-programmed reduction (TPR) and temperature-programmed oxidation (TPO) experiments were carried out in a semiautomatic Micromeritics TPD/TPR 2900 apparatus interfaced to a microcomputer. TPR profiles were obtained by passing a 10% H_2/Ar flow (50 cm^3/min) through the sample. The temperature was increased from 323 to 1046 K at a rate of 10 K/min, and the amount of H_2 consumed was determined with a TCD; the effluent gas was passed through a cold trap placed before the TCD in order to remove water from the exit stream. TPO profiles were recorded in a similar way. For this, the reduced catalysts were cooled to ambient temperature in a He flow and then exposed to a 3% O_2/He flow (50 cm^3/min) while increasing the temperature at a rate of 10 K/min up to a final temperature of 1200 K.

The cobalt metal surface area was determined by hydrogen chemisorption measurements were obtained in a conventional pyrex glass volumetric adsorption apparatus. A 200-mg sample of the perovskite was reduced at 1250 K for 3.5 h under a stream of 33% H_2/N_2 and then outgassed at 773 K overnight at pressures lower than 10^{-4} Torr (1 Torr = 133.3 Pa). The adsorption isotherms were measured at 313 K after 2 h equilibration at this temperature. This temperature was used since the chemisorption process is known to be highly activated on cobalt (22). The total amount of chemisorbed H atoms was used to determine the number of vacant Co° atoms at the surface using the stoichiometry $H/Co_s = 1$ (22). The reproducibility was within 10%.

X-ray photoelectron spectra were acquired with an ESCALAB 200R spectrometer equipped with a Mg$K\alpha$ 120-W X-ray source (hv = 1253.6 eV). Both H_2-reduced and used catalysts were analyzed by XPS. The prereduced catalysts in H_2 flow at 1023 K for 3.5 h and then used in the reaction were all quenched to room temperature under argon and immediately drenched in isooctane. Despite this careful procedure to isolate the catalyst it was not possible to completely avoid oxidation of the surface metallic cobalt during transferral of the sample from the reactor to the XPS spectrometer. The samples were pressed into small aluminum cylinders and then mounted on a sample rod placed in a pretreatment chamber and outgassed at room temperature for 1 h prior to being transferred to the analysis chamber. The pressure in the ion-pumped analysis chamber was below 3×10^{-9} Torr during data acquisition. The spectra were collected for 20 to 90 min, depending on the peak intensities, at a pass energy of 10 eV (1 eV = 1.602×10^{-19} J). The intensities were estimated by calculating the integral of each peak after smoothing and subtraction of the S-shaped background and fitting the experimental curve to a combination of Gaussian and Lorentzian lines of variable proportion. All binding energies (BE) were referenced to the adventitious C 1s line at 284.9 eV. This reference gave BE values within an acuracy of ±0.1 eV.

Temperature-programmed desorption (TPD) experiments were performed on aliquots of catalysts (50 mg) placed in a quartz reactor attached to a vacuum line and gas handling system. The samples were reduced as described above and outgassed at 773 K for typically 3 h until no desorption from the catalyst was observed by the MS detector. Subsequently, they were cooled down to 313 K and exposed to a 100-Torr CO pulse for 15 min. Once the gas phase was removed, the samples were heated to 1073 K at a constant heating rate of 5 K/min and the desorbing species were monitored with a MS detector. A Balzers QMA 125 quadrupole mass spectrometer, capable of monitoring 16 masses simultaneously, connected in line with the reactor, was used for the analysis of the desorption products.

The catalytic tests were carried out in a quartz fix bed flow microreactor (4 mm inner diameter). A space velocity (HGSV) of 2×10^5 h^{-1} and a mixture $CH_4/O_2/Ar = 2:1:4$ (molar ratio) at a flow rate of 166.6 cm^3/min were used. The catalyst weight (50 mg) was held in the middle of the reactor using quartz wool. Flow rates were controlled by Unit mass flow controllers. All the catalyst were reduced *in situ* with a 33% H_2/Ar mixture (50 cm^3/min) at 1023 K for 3.5 h prior the reaction. After the reduction, the H_2 flow was stopped and the flows of methane and argon adjusted for the reaction. The oxygen was then slowly introduced, producing an increase in the bed temperature due to exothermic oxidation reactions. Two thermocouples were used, one outside the reactor to control the furnace temperature and the other one inside in contact with the catalyst through a quartz sheath to measure the bed temperature. The effluents of the reactor were sampled by means of a six-port valve and then analyzed on-line by GC (Hewlett Packard HP 5890), using Ar as the carrier, which allowed direct analysis of hydrogen and other products.

3. RESULTS

3.1. Catalyst Characterization

The temperature programmed reduction profiles of the cobalt containing perovskites are displayed in Fig. 1. All the perovskites showed similar reduction profiles consisting of two sets of peaks at approximately 633 and 833 K. It can be observed that especially for $LaCoO_3$ and $PrCoO_3$ the second reduction peak shifts to higher temperatures. For example, the reduction peak for $SmCoO_3$ at ca. 785 K is observed at 844 K for $LaCoO_3$. In all cases the hydrogen consumption for the first reduction step (peak at ca. 633 K) was always approximately half of the hydrogen consumption obtained for the second reduction step (peak at 833 K). Careful thermogravimetric reduction experiments (not shown here) demonstrated that the first step is a one-electron reduction process ($Co^{3+} + e \rightarrow Co^{2+}$) whereas the second step is a two-electron reduction process ($Co^{2+} + 2\,e \rightarrow Co^{\circ}$). TPR profiles of the first step of reduction display a long tail in the lower temperature of reduction and split in two components, indicating that the reduction process is activated and probably controlled by mass transport of H_2 or/and H_2O across the lattice.

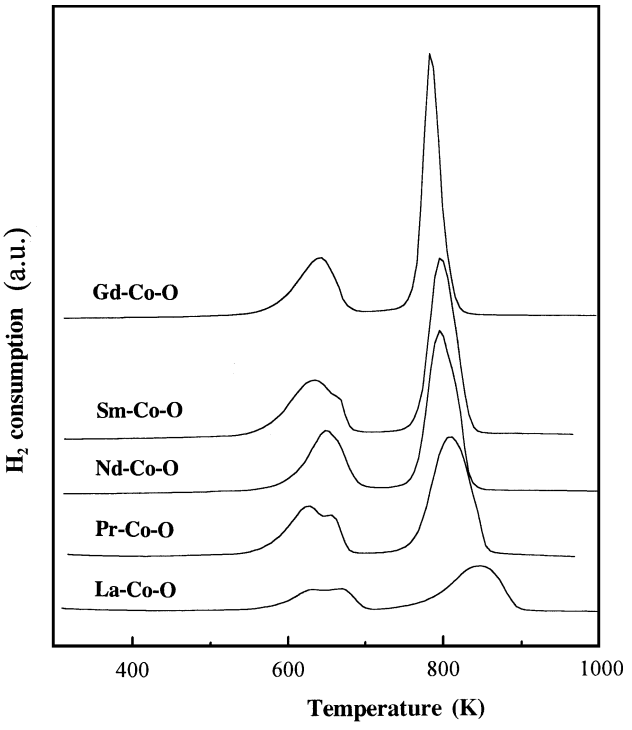

FIG. 1. Temperature-programmed reduction profiles of $LnCoO_3$ perovskite oxide precursors.

To identify the reduced species formed in the TPR steps in Fig. 1 XRD studies of $NdCoO_3$ subjected to different reduction treatments were carried out (Fig. 2). The XRD pattern displayed in Fig. 2a corresponds to $NdCoO_3$ cubic perovskite structure. Upon reduction at 623 K under H_2 flow for 15 min the diffraction peaks are essentially at the same position but with a very strong broadening and in some peaks a splitting is observed (Fig. 2b). This indicates that the perovskite structure is basically the same, however distorted due to the creation of anion vacancies. These results suggest that the stoichiometry of the phase formed in the first step 1 electron reduction can be represented as $NdCoO_{2.5}$. The reoxidation of this sample at 973 K under oxygen flow can easily regenerate the original perovskite structure (XRD not shown here), demonstrating the reversibility of this process. On the other hand, the phase $NdCoO_{2.5}$ is not stable and at high temperatures (1123 K for 1 h) under He phases of CoO and Nd_2O_3 hexagonal are formed (Fig. 2c). When the perovskite was treated with hydrogen at 778 K for 15 min, a three-electron reduction was observed and XRD analysis showed the presence of Nd_2O_3 hexagonal and very weak and broad peaks which could be due to metallic cobalt (Fig. 2d). Upon heating at 1123 K in helium the highly dispersed cobalt metal sinters

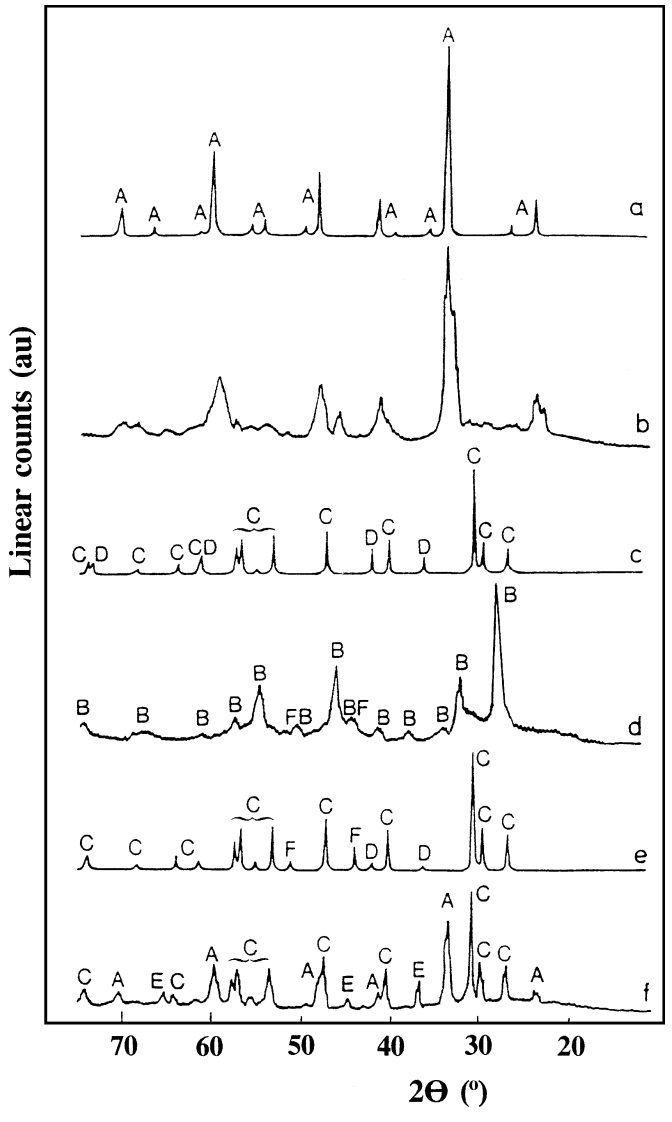

FIG. 2. Powder X-ray diffraction patterns for $NdCoO_3$: (a) as prepared, (b) reduced in hydrogen at 623 K for 15 min, (c) after reduction (623 K, 15 min) and heated under He at 1123 K for 1 h (sintering), (d) reduced in hydrogen at 778 K for 15 min, (e) after reduction (778 K, 15 min) and sintering, (f) after reduction (778 K, 15 min), sintering at 1123 K and reoxidation under O_2 flow at 973 K. A, $NdCoO_3$; B, Nd_2O_3 (cub); C, Nd_2O_3 (hex); D, CoO; E, Co_3O_4; and F, Co°.

and shows much stronger lines in the XRD pattern (Fig. 2e). The presence of small amounts of CoO, probably formed by the reoxidation of cobalt by water or oxygen still present in the sample during sintering, was also observed. The reoxidation of the reduced sample in Fig. 2d (before sintering) also reproduced the perovskite original structure with the same XRD pattern (not shown here). However, after sintering (Fig. 2f) the reoxidation produces a mixture of the phases $NdCoO_3$, Co_3O_4, and Nd_2O_3 (Fig. 2f), showing that the process is not completely reversible. It was observed that if the sample in Fig. 2f was kept under oxygen flow at temperatures of 1123 K for 1 h a slow solid state reaction takes place regenerating the perovskite $NdCoO_3$ structure. Therefore, the two main reduction steps of $NdCoO_3$ can be written as:

$$1\ \text{e/mol: } 2\,NdCoO_3 + H_2 \rightleftarrows 2\,NdCoO_{2.5} + H_2O \quad [2]$$

$$3\ \text{e/mol: } 2\,NdCoO_3 + 3H_2 \rightleftarrows Nd_2O_3 + 2Co^\circ + 3H_2O. \quad [3]$$

These reactions are reversible and as long as the metallic cobalt remains well dispersed the perovskite structure can be easily regenerated by oxidation. These results are in agreement with the work of Crespin and Hall (23), who observed basically the same reduction steps for $LaCoO_3$.

The cobalt metal area of the reduced perovskites was determined by hydrogen chemisorption experiments. The results are shown in Table 1. The chemisorption measurements revealed that the cobalt metallic surface area was similar for all the perovskites. This is supported by the Co/Ln surface ratio (Table 1) obtained by XPS which also suggests similar metallic dispersion. The XPS analyses of the reduced perovskites showed the presence of Co° (778.6 eV) but also a doublet at approximately 780.5 and 796.2 eV which correspond to Co $2p_{3/2}$ and Co $2p_{1/2}$, respectively, for the Co^{3+} ion (Fig. 9A). It can be also noted in Fig. 9A that the intensity of the component at approximately 778.6 eV, associated to the metallic cobalt, does not change substantially from catalyst to catalyst. As can be seen below, this is not the case for the catalyst used in which the proportion of reduced cobalt (Co°) decreased dramatically or even disappeared (see Fig. 9B). Shake-up satellite lines with 4.7 eV over the Co^{3+} lines were also detected, indicating the presence of Co^{2+} (24). These oxidized species of cobalt are probably formed by air oxidation during the transferral of the reduced sample from the reactor to the XPS spectrometer. Also, Marcos *et al.* (25) have shown that the reduction of the perovskite $LaCoO_3$ produced a La_2O_3 oxide covered by hydroxyl groups which, upon heating and evacuation in the XPS chamber, partly reoxidizes the cobalt crystallites.

TABLE 1

Characterization of the Reduced Perovskites

Precursor	BET area (m^2/g) perovskite	BET area (m^2/g) (red. cat.)	Co° area (Co° atoms/g) (red. cat.)	Co/Ln ratio by XPS[a] (red. cat.)	XRD (red. cat.)
$LaCoO_3$	8.6	5.4	3.77×10^{19}	0.71	La_2O_3 (hex)
$NdCoO_3$	5.6	4.5	3.98×10^{19}	0.50	Nd_2O_3 (hex)
$SmCoO_3$	5.1	—	3.69×10^{19}	0.58	Sm_2O_3 (cub)
$GdCoO_3$	4.0	5.0	3.21×10^{19}	0.75	Gd_2O_3 (cub)

Note. red. cat., catalysts reduced at 1023 K under 33% H_2/Ar flow for 3.5 h.

[a] For the XPS Co/Ln ratio determination all cobalt signals (metal, oxidized forms, and shake-up satellite lines) were included.

Powder XRD analysis of the reduced $LnCoO_3$ perovskites showed only the presence of the sesquioxides La_2O_3 (hex), Nd_2O_3 (hex), Sm_2O_3 (cub), and Gd_2O_3 (cub). The apparent absence of reflections for the metallic cobalt indicates a high metallic dispersion with Co° particles smaller than 2 nm. Considering the approximate value of 3×10^{19} atoms/m^2 for a close packing arrangement (26), the number of surface cobalt metallic atoms obtained for the reduced catalysts is similar to the number of surface cobalt ions on the original perovskite surface (between 2×10^{19} to 5×10^{19} atoms/g for $GdCoO_3$ with BET surface area of 4.0 m^2/g and $LaCoO_3$ 8.6 m^2/g, respectively). It therefore seems that after reduction of the perovskites a large proportion of the cobalt metal is located in the bulk of the material.

Temperature-programmed oxidation analyses were performed for the reduced catalysts in order to investigate the stability of these systems toward gas phase oxygen (Fig. 3). The perovskites were completely reduced in a TPR experiment with a stream of 10% H_2 in Ar heating from room temperature to 923 K at a rate of 10 K/min. The temperature was then rapidly decreased to avoid sintering of the cobalt metal and TPO analysis performed. TPO profiles showed that the oxidation takes place in two steps. The first one at near 473 K (peak I) has an oxygen consumption which suggests that the cobalt is oxidized to two Co^{3+} and one Co^{2+}. Therefore, this oxidation probably corresponds to the formation of the cobalt oxide spinel according to the reaction.

$$3Co^\circ + 2O_2 \rightleftarrows Co_3O_4. \qquad [4]$$

The second step (peak II) takes place at a much higher temperature and the oxygen consumption suggests the following process:

$$Co_3O_4 + 1/4\,O_2 + 3\,Ln_2O_3 \rightleftarrows LnCoO_3 \qquad [5]$$

In this step apparently the Co^{2+} is oxidized to Co^{3+} simultaneously with a solid state reaction to regenerate the perovskite structure. The occurrence of these reactions are also supported by simple experiments involving sequences of TPO and TPR measurements, shown in Figs. 4A and 4B. It can be observed that the TPR profile, obtained with the sample reduced in the first TPR (Fig. 4B, profile a), and reoxidised in the first TPO up to 1123 K (Fig. 4A, profile a), is very similar to the TPR of the fresh sample (Fig. 4B, profile a), suggesting the presence of a $SmCoO_3$ perovskite structure. On the other hand, if the reduced sample, after a complete reduction–oxidation cycle, is then reoxidized in a TPO experiment, which is interrupted at 623 K (Fig. 4A, profile b), and the sample heated up to 1123 K under He, the TPR analysis shows only a broad peak at ca. 623 K (Fig. 4A, profile c), which is similar to the reduction of the spinel Co_3O_4 reported in the literature (27).

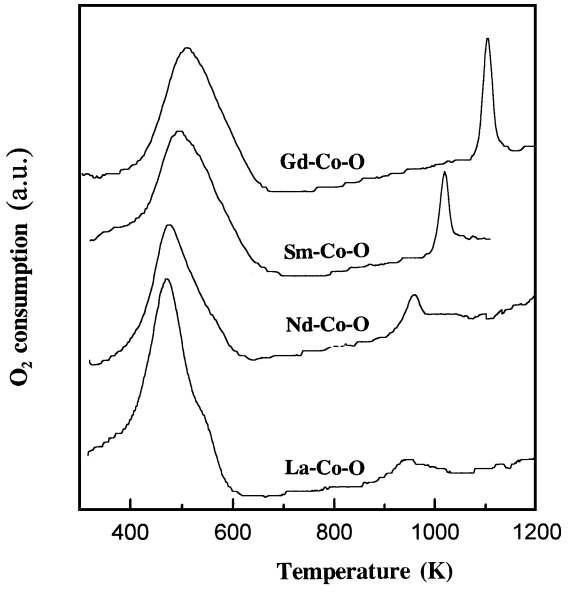

FIG. 3. Temperature-programmed oxidation profiles for the reduced La–Co–O, Nd–Co–O, Sm–Co–O, and Gd–Co–O catalyst systems.

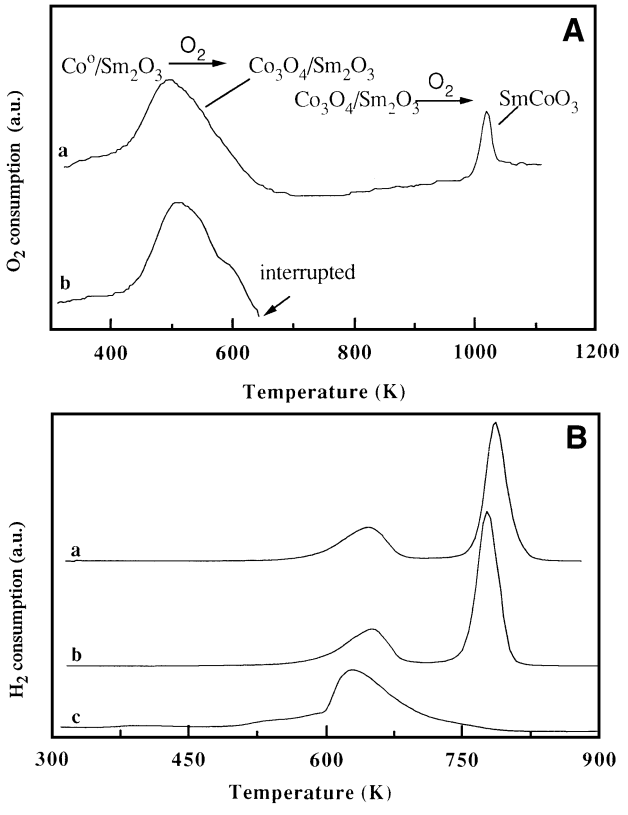

FIG. 4. (A) TPO profiles of the Sm–Co–O system: (a) sample prereduced at 900 K and then reoxidized at 1123 K, (b) after cycle (a) reduced at 900 K and subsequently oxidized at 623 K. (B) TPR profiles of the Sm–Co–O system: (a) original sample reduced at 900 K, (b) sample (a) reoxidized at 1123 K followed by reduction at 900 K, (c) sample (b) reoxidized at 623 K and then heated at 1123 K under He, followed by reduction at 900 K.

It is interesting to note in Fig. 3 that the temperature for the first oxidation step is similar for all the catalysts whereas the temperature of the second step is strongly dependent on the nature of the lanthanide. For lanthanum, oxidation occurs at 939 K, whereas for gadolinium a much higher temperature is necessary (1109 K). Also the area and the shape of the second peak varied significantly for the different lanthanides. Very sharp peaks were obtained for Gd and Sm, whereas a broad and weak peak was observed for La. The $A_{\text{peak I}}/A_{\text{peak II}}$ area ratio of the first and the second peak from the TPO profiles shown in Fig. 3 are 12.5, 10.0, 9.0, and 7.5 for La–Co–O, Nd–Co–O, Sm–Co–O, and Gd–Co–O, respectively. The systems La–Co–O and Nd–Co–O can be observed to deviate significantly from the expected area ratio which is 8.0 considering the stoichiometry of Eqs. [4] and [5]. This suggests that part of the cobalt which in the Gd–Co–O and Sm–Co–O systems is oxidized only at temperatures higher than 973 K, is being oxidized at lower temperatures for La–Co–O and Nd–Co–O. In fact, Crespin *et al.* (23) showed that if the reduced $LaCoO_3$ was kept at a temperature as low as 673 K under oxygen the metallic cobalt was completely reoxidized, regenerating the perovskite structure.

3.2. Carbon Monoxide TPD Experiments

Figures 5A–5C display TPD profiles of CO adsorbed on the reduced systems La–Co–O, Nd–Co–O, and Gd–Co–O, respectively. In Fig. 5A, the presence of basically two peaks of CO can be observed, peak I at ca. 453 K and peak II at ca. 693 K. Cortes and Droguett (28) studied cobalt supported on kieselguhr and also obtained a CO TPD with two peaks at very similar temperatures which they assigned to surface Co-linear carbonyl species (peak I) and Co-bridged carbonyl (peak II). Further TPD and IR studies were then reported in the literature supporting the linear and bridged assignments of these CO TPD peaks (29–31). Figure 5A shows that the intensity of CO peak I is similar for all the systems studied, La–Co–O, Nd–Co–O, and Gd–Co–O. On the other hand, it can be clearly seen that the CO peak II for La–Co–O almost disappears while it increases in intensity for Nd–Co–O and especially for Gd–Co–O. As observed in Fig. 5B, desorption of the CO peak II is accompanied by the formation of significant amounts of CO_2. This CO_2 is probably produced during CO TPD by the disproportionation of CO,

$$2\,CO_{surf} \rightleftarrows CO_2 + C_{surf}, \qquad [6]$$

and/or by the reaction of CO with superficial hydroxyl groups (32–34),

$$CO_{surf} + OH_{surf} \rightleftarrows CO_2 + 1/2\,H_2. \qquad [7]$$

No H_2O was observed in TPD blank experiments with the catalysts La–Co–O, Nd–Co–O, and Gd–Co–O, which precludes the possibility of the water gas shift reaction as a source of H_2 and CO_2. Two differences are noted in the CO_2 signals in Fig. 5B. The first one is that relatively large amounts of CO_2 are produced for the La–Co–O system, decreasing for Nd–Co–O, and very little is produced for Gd–Co–O. The second feature is the desorption temperature of CO_2, which increases in the order La > Nd > Gd. In Fig. 5C it is observed that also hydrogen ($m/e = 2$) is produced in large amounts for La–Co–O compared to that seen with Nd–Co–O and Gd–Co–O. These results seem to suggest that the reaction with surface hydroxyl groups described in Eq. [7] is present during the CO TPD experiments. In this respect, the basicity of the rare earth oxides, which decreases in the order $La_2O_3 > Nd_2O_3 > Gd_2O_3$ (35, 36), might play an important role in the reaction. For example, due to its strong basicity, La_2O_3 is known to form very high concentrations of stable hydroxyls and oxycarbonate species in a wide temperature range (24, 25, 37–40). LaO(OH) decomposes to form La_2O_3 only at temperatures higher than 800 K (38). Therefore, these hydroxyl groups

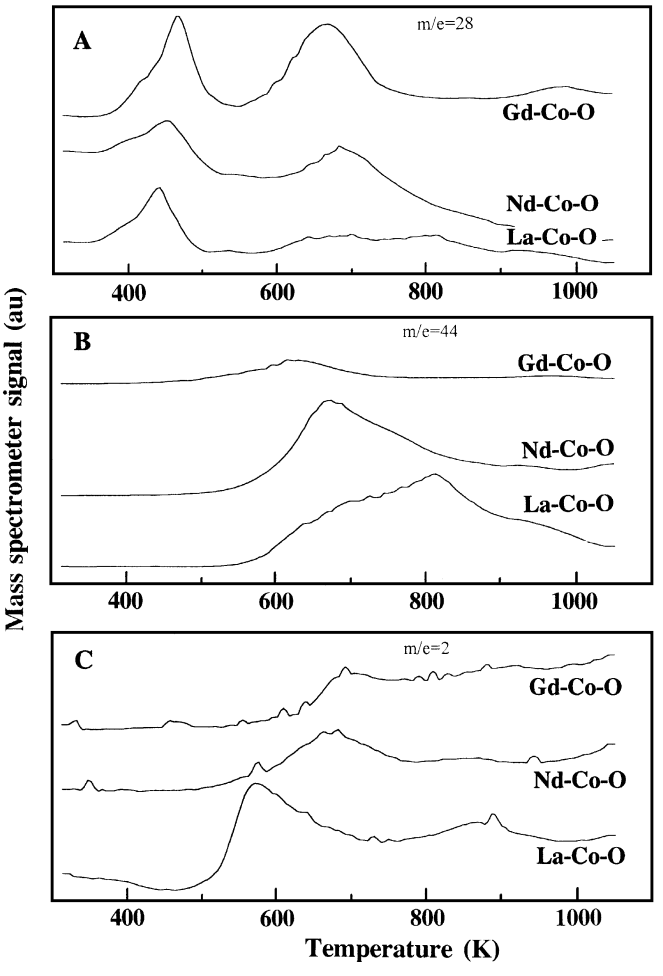

FIG. 5. Temperature-programmed desorption profiles of CO from the reduced La–Co–O, Nd–Co–O, and Gd–Co–O catalysts: (A) CO ($m/e = 28$), (B) CO_2 ($m/e = 44$), and (C) H_2 ($m/e = 2$).

on the surface of La_2O_3 react with CO desorbing during the TPD in peak II (Fig. 5A) producing CO_2 and H_2. The higher desorption temperature of CO_2 observed in the TPD for La–Co–O (Fig. 5B) might be related to the basicity of La_2O_3 which results in a stronger interaction with the acid molecule CO_2. In the case of the Gd–Co–O system where the Gd_2O_3 oxide is less basic, a relatively low concentration of hydroxyl groups is probably produced and therefore the presence of the reaction described in Eq. [7] is considerably diminished. The CO disproportionation (Eq. [6]) during the TPD experiments has not been investigated in this work and a more detailed study is necessary to comment on it. TPD studies on Rh supported on silica promoted with La_2O_3 (32, 41) suggested that although the disproportionation of CO was present, the contribution of Eq. [7] to the formation of CO_2 was much more important.

3.3. *Catalytic Testing*

Among the cobalt containing perovskites, $GdCoO_3$, $SmCoO_3$, $NdCoO_3$, $PrCoO_3$, and $LaCoO_3$, tested as catalyst precursors for the partial oxidation of methane, the Gd–Co–O system showed exceptionally better performance for synthesis gas formation (Figs. 6A–6C). At 1009 K a steady-state methane conversion of 73% with selectivities of 79 and 81% for CO and H_2, respectively, is observed for the catalyst Gd–Co–O. The catalysts Sm–Co–O and Nd–Co–O, of lower activity, show similar steady-state methane conversions in the temperature range studied. On the other hand, the H_2 and CO selectivities are much higher over Sm–Co–O.

The catalyst La–Co–O is active for the methane combustion and only traces of H_2 and CO were observed under the reaction conditions used (Figs. 6A–6C). It is interesting to observe that, at a constant temperature, the steady-state yields of H_2 and CO followed inversely the order of the ionic radii of the rare earth (Fig. 7), considering the oxidation state +3, coordination number 8, and the sesquioxides of structural type A for La_2O_3, Pr_2O_3, and Nd_2O_3 and type B for Sm_2O_3 and Gd_2O_3 (42). Therefore, the gadolinium which has the shortest ionic radius shows the highest CO and H_2 yields. On the other hand, for the catalyst containing lanthanum (the largest ion) no syngas formation was observed (Fig. 7).

All the catalytically active systems for syngas production showed hysteresis behavior. Figures 8A–8C display the hystereses observed in the methane conversion and H_2 and CO selectivities over the catalysts Gd–Co–O, Sm–Co–O, and Nd–Co–O. When the reaction temperature over the prereduced catalyst was increased from ca. 823 K up to ca. 1073 K the conversion of methane and selectivities for CO and H_2 also increased. However, if the reaction temperature was then decreased the observed conversion and selectivities were always higher than the values obtained when the temperature had been increased.

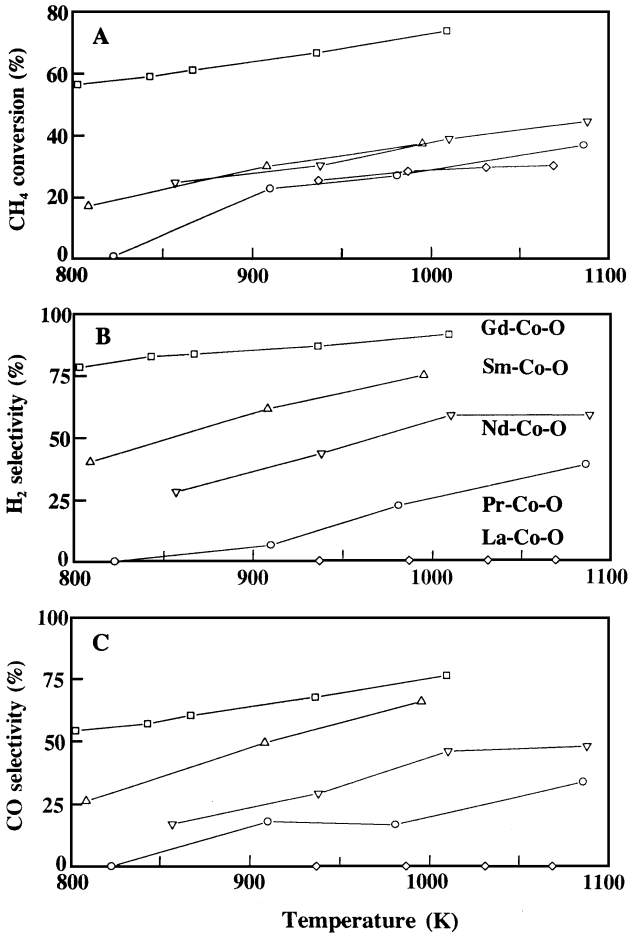

FIG. 6. (A) Methane conversion and (B) H_2 and (C) CO selectivities in the presence of Ln–Co–O systems prereduced under a 30% H_2/Ar flow at 1023 K for 3.5 h.

3.4. *Characterization of Used Catalysts*

XPS studies were further carried out to know the oxidation state of cobalt in the catalysts after on-stream process. The La–Co–O catalyst after reaction at 1023 K for 19 h showed the Co 2p spin-orbit splitting at 780.5 and 796.2 eV, which correspond to Co $2p_{3/2}$ and Co $2p_{1/2}$ levels,

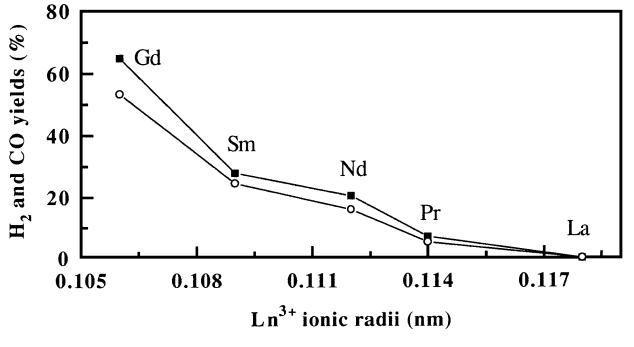

FIG. 7. Steady-state H_2 (■) and CO (◯) yields as a function of the lanthanide ionic radii.

respectively, for the Co^{3+} ion. Moreover, the observation of shake-up satelite lines with approximately 4.7 eV over the Co^{3+} indicates the presence of Co^{2+} (23). No line at 778.6 eV was observed, suggesting the absence of metallic cobalt on the surface (Fig. 9B, spectrum a). The Co $2p_{3/2}$ core-level spectra of catalysts Gd–Co–O, Sm–Co–O, and Nd–Co–O after reaction showed the lines at 778.6 and 780.3 eV, indicating the presence of both metallic cobalt and oxidized forms of cobalt, respectively, on the surface of the used catalysts (Fig. 9B). The XPS Co/Ln ratios determined (including the satellite lines for both Co $2p_{3/2}$ and the lanthanide) shown in Table 2 suggest that the cobalt dispersion over the catalyst surface after reaction follows the order La–Co–O > Gd–Co–O > Sm–Co–O > Nd–Co–O.

XRD analyses of the used catalysts Gd–Co–O and Sm–Co–O showed similar patterns to the reduced catalysts. Very strong and sharp peaks for the sesquioxides Gd_2O_3 (Fig. 10A) and Sm_2O_3 can be observed. On the other hand, XRD analysis of the La–Co–O catalyst after reaction at 1023 K for 19 h clearly showed the formation of the perovskite $LaCoO_3$ (Fig. 10B). The XRD for Nd–Co–O after reaction revealed the presence of the phases Nd_2O_3 and also the perovskite $NdCoO_3$ (Fig. 10C). For all used catalysts no clear evidence for the presence of simple cobalt oxides such as CoO, Co_2O_3, and Co_3O_4 could be found by XRD.

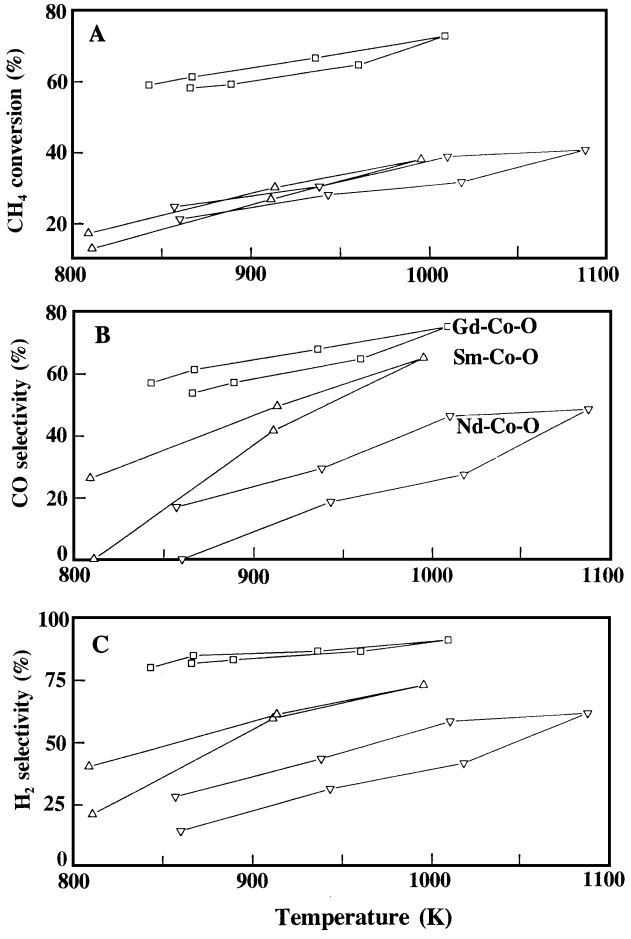

FIG. 8. Effect of the reaction temperature on the (A) methane conversion and (B) H_2 and (C) CO selectivities over prereduced $GdCoO_3$, $SmCoO_3$, and $NdCoO_3$ perovskite precursors.

TABLE 2

XRD and XPS Analyses of the Catalyst after On-Stream Operation[a]

Precursor	Co/Ln surface ratio by XPS[b]	Crystalline phases (XRD)
$LaCoO_3$	0.7	$LaCoO_3$ La_2O_3 (tr)
$NdCoO_3$	0.2	Nd_2O_3 (hex) $NdCoO_3$
$SmCoO_3$	0.3	Sm_2O_3 (cub)
$GdCoO_3$	0.5	Gd_2O_3 (cub)

Note. tr, traces; hex, cub, the hexagonal and cubic crystalline phases, respectively.

[a] Reaction at 1023 K for 19 h.

[b] For the Co/Ln signal ratio determination all cobalt signals, metal, oxidized forms, and shake-up satellite lines were included.

For the reduced perovskites $NdCoO_3$ and $GdCoO_3$ the Nd_2O_3 (hex) and Gd_2O_3 (cub) phases were observed. Coincidentally, the strong diffraction lines of the metallic cobalt planes (101), (110), (103), and (112) with interplanar distances of 0.1910, 0.1252, 0.1149, and 0.1066 nm, respectively, are also observed for the oxides of gadolinium, samarium, and neodymiun. Therefore, it was not possible to obtain information about the metallic particles from the XRD analyses.

4. DISCUSSION

According to the powder XRD analyses reduction of the perovskite precursors produced metallic cobalt dispersed on the rare earth sesquioxides, Co°/Ln_2O_3. The results reported in the literature (8–10) suggest that metallic cobalt is probably the active phase for the oxidation of methane to synthesis gas. It is interesting to observe that, although the reduced perovskites possess similar cobalt metallic surface area as revealed by H_2 chemisorption and XPS data, they showed strikingly different catalytic properties. For example, the catalyst Gd–Co–O showed very high activity for synthesis gas formation, whereas La–Co–O produced only CO_2 and H_2O.

In the case of the La–Co–O system, the XRD and XPS results showed that under the reaction conditions studied the metallic cobalt is reoxidized back, producing the original perovskite structure $LaCoO_3$. Therefore, it is not surprising that the only reaction products observed were water and carbon dioxide. This agrees with previous works on this perovskite and other forms of cobalt oxide which have been shown to be active catalysts for methane combustion and

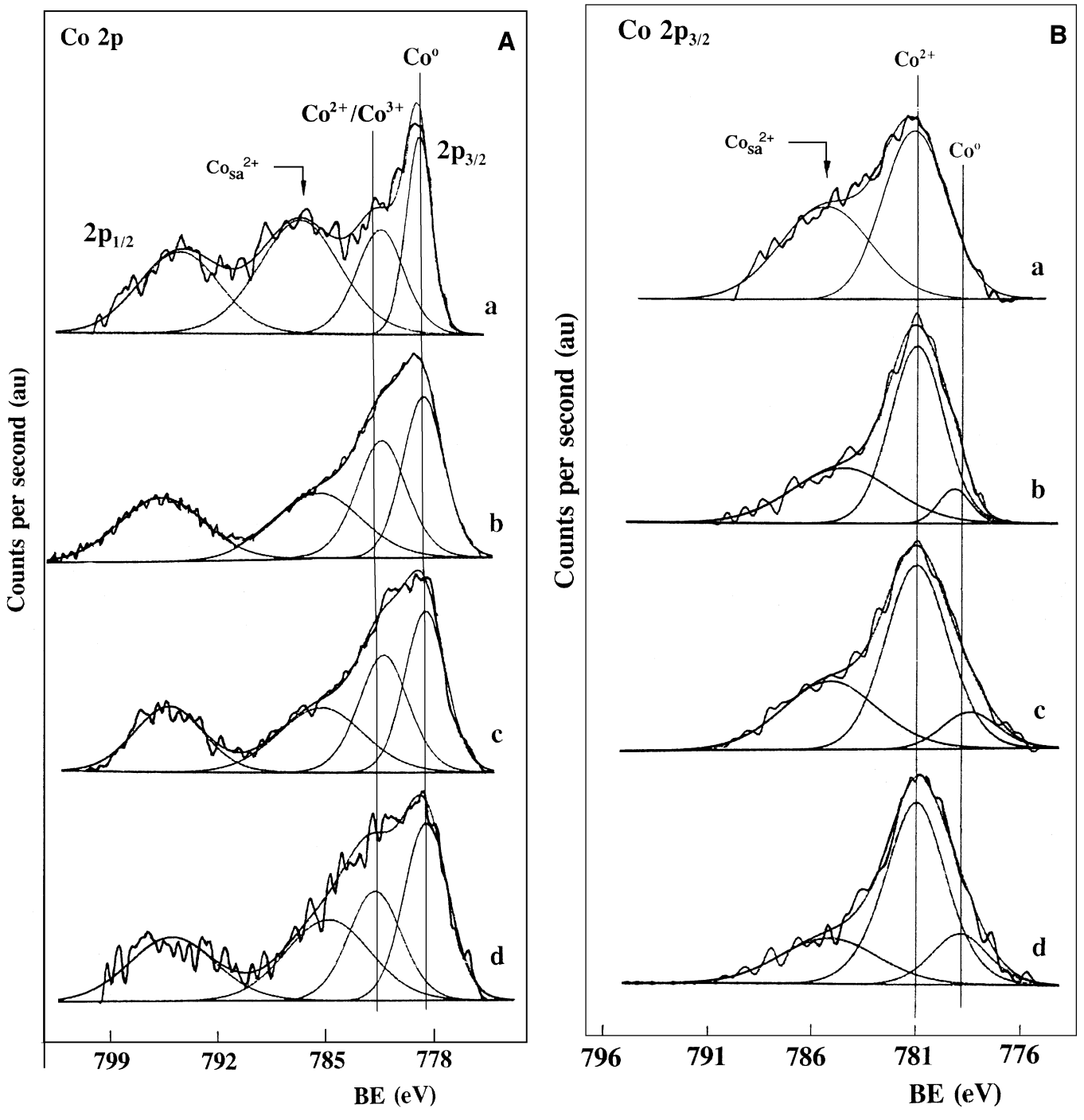

FIG. 9. Co $2p_{3/2}$ core level spectra of (A) reduced $LnCoO_3$ (under a 30% H_2/Ar flow at 1023 K for 3.5 h) and (B) used (reaction at 1023 K for 19 h) catalysts. (a) La–Co–O, (b) Nd–Co–O, (c) Sm–Co–O, and (d) Gd–Co–O.

also for CO and H_2 oxidation (43). The high Co/Ln surface ratio determined by XPS for the used catalyst is expected for a perovskite-like surface. Slagten and Olsbye (9) studied the perovskite $LaCoO_3$ (containing some impurities of La_2O_3 and Co_3O_4) for the partial oxidation of methane to syngas and observed the production of mainly CO_2. If the catalyst was kept at 1073 K after 30 h on-stream the activity changed to give mainly CO which they assigned to the *in situ* reduction of cobalt.

The used catalyst Nd–Co–O shows fairly high amounts of the perovskite $NdCoO_3$ formed during the reaction. This perovskite promotes the nonselective oxidation of methane and also CO and H_2. On the other hand, the Gd–Co–O and Sm–Co–O systems, which showed the best

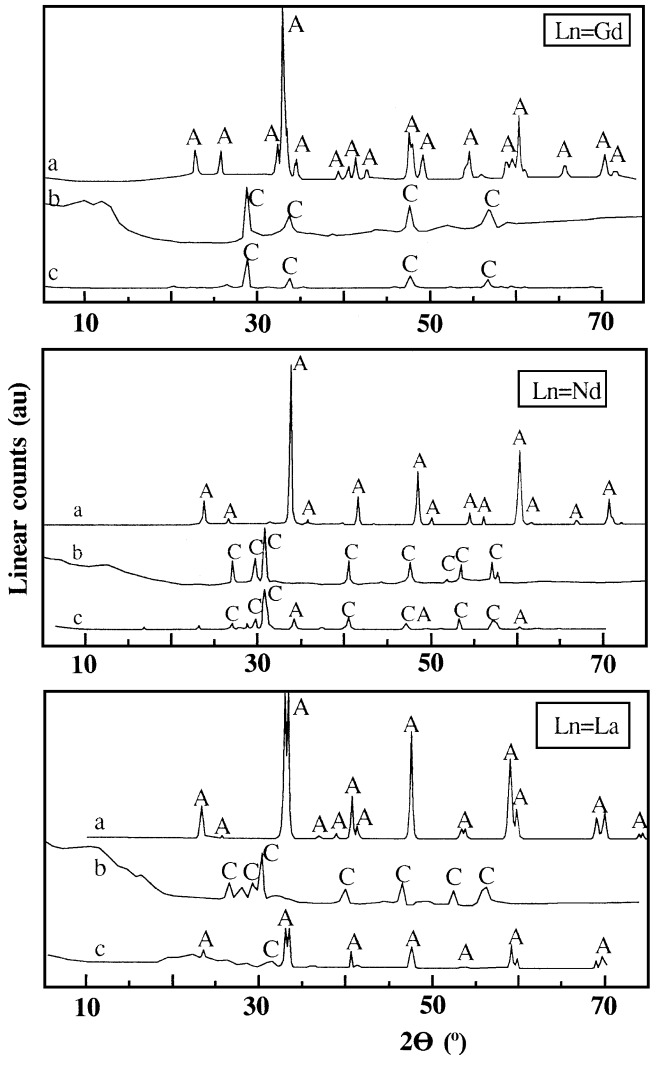

FIG. 10. X-ray diffraction patterns for (a) calcined perovskite precursors $LnCoO_3$, (b) after reduction (under a 30% H_2/Ar flow at 1023 K for 3.5 h), and (c) after reaction (1023 K for 19 h). A, $LnCoO_3$; C, Ln_2O_3.

performances for syngas production, under reaction did not reoxidize back to the original perovskites. According to the XPS Co/Ln surface ratio (Table 1), the Gd–Co–O catalyst shows a cobalt dispersion (Co/Ln = 0.75) higher than that of Sm–Co–O (0.58) which may be responsible for the different activities of these catalysts. These phase transformations involving the perovskite and the simple oxides under oxidative and reductive conditions have been carefully studied by XRD for $NdCoO_3$. $NdCoO_3$ was observed to be consecutively reduced first to $NdCoO_{2.5}$ and then to metallic cobalt dispersed over Nd_2O_3. These two reduced forms in the presence of oxygen at high temperature were demonstrated to be easily reoxidized back to the perovskite structure. However, if the metallic cobalt is sintered the reoxidation is not completely reversible, producing a mixture of $NdCoO_3$, Nd_2O_3, and CoO. Similar results for $LaNiO_3$ and $LaCoO_3$ have been reported in the literature (44–47).

The hysteresis behavior observed for the Co–Ln–O catalysts (except La–Co–O) (Figs. 8A–8C) has been discussed for alumina supported nickel catalysts during the partial oxidation of methane (6, 7). Lunsford *et al.* (6), using XRD and XPS, demonstrated that only for reaction temperatures higher than 973 K is the precalcined $NiAl_2O_4$ reduced to produce metallic nickel which is active for syngas formation. Decreasing the temperature to 673 K, the oxygen consumption is not complete and all the surface nickel is oxidized back to the spinel $NiAl_2O_4$. Apparently, a similar process occurs in our catalytic systems. At low reaction temperatures, where the oxygen conversions are lower, oxidation of the surface metallic cobalt takes place. These oxidized forms of cobalt are active for the total oxidation of methane and also for the oxidation of CO and H_2 formed during the reaction. At reaction temperatures as high as 1023 K the oxygen conversion is complete (for Gd–Co–O) or almost complete, so a reducing atmosphere is produced. In this situation the Co° is favored and an increase in the selectivities for syngas is observed. If the temperature is then decreased the metallic cobalt is slowly reoxidized and the H_2 and CO selectivities also decrease. Also, with an increase in the reaction temperature, the Co° present in the bulk of the catalyst may migrate, causing an increase in catalytic activity.

As observed by TPR, the nature of the Ln affects the reducibility of Co in the perovskites $LnCoO_3$. The Goldschmidt tolerance factor $t = (r_{Ln} + r_O)/[\sqrt{2}(r_{Co} + r_O)]$ obtained for the structures of $LaCoO_3$, $PrCoO_3$, $NdCoO_3$, $SmCoO_3$, and $GdCoO_3$ were 0.899, 0.885, 0.878, 0.867, and 0.857, respectively. These tolerance factors indicate that considering solely geometric factors lanthanum, the largest ion in the series, forms the most stable perovskite structure. This trend is reflected in the TPR results, where the perovskite $LaCoO_3$, the most stable structure, is reduced at the higher temperatures, 844 K (Fig. 11).

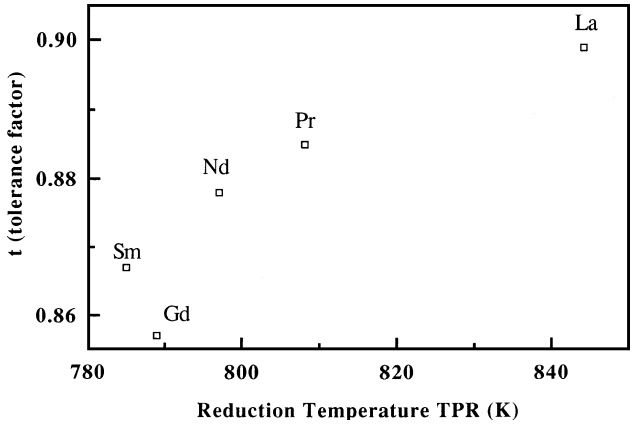

FIG. 11. Goldschmidt's tolerance factor *t* and reduction temperature obtained from temperature-programmed reduction experiments for the $LnCoO_3$ perovskites.

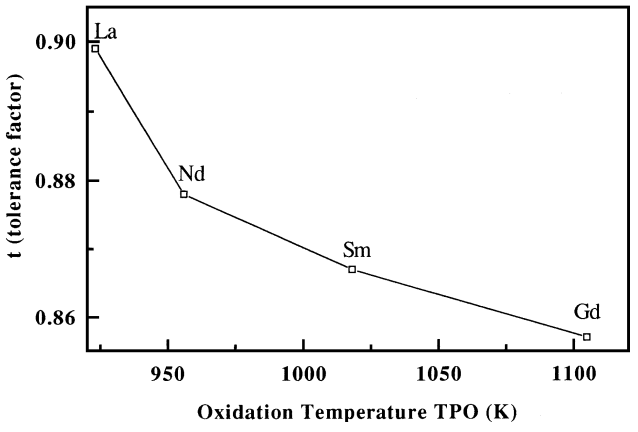

FIG. 12. Goldschmidt's tolerance factor t and oxidation temperature obtained from temperature-programmed oxidation experiments for the $LnCoO_3$ perovskites.

Likewise, the TPO experiments showed that reoxidation of cobalt to form the perovskite structure is more favorable for larger lanthanides. Figure 12 shows a good correlation between the oxidation temperature obtained from the TPO profiles and the Goldschmidt tolerance factor. Katsura *et al.* (48) studied the thermodynamics of the oxidation of iron to the rare earth perovskites between 1473 and 1673 K according to the reaction

$$Fe\,(s) + 1/2\,Ln_2O_3 + 3/4\,O_2\,(g) \rightleftarrows LnFeO_3\,(s). \quad [8]$$

They showed that reoxidation to form the perovskite structure is favored in the order La > Nd > Sm > Gd with standard Gibbs energies of −288.0, −274.6, −267.9, and −263.7 kJ/mol, respectively.

The question of whether, under reaction conditions, other factors affect the stability and activity of the catalysts is under investigation. For example, the basicity of the rare earth oxides which increases in the order Gd < Sm < Nd < Pr < La is known to have a strong effect on the oxidative coupling of methane (35, 36). Marcos *et al.* (25) studied the reduced perovskites $La_{1-y}A_yCoO_3$ (A = Sr and Th) and showed that at increasing oxide basicities, Sr > La > Th, the surface becomes covered by hydroxyls. They demonstrated that upon heating in a vacuum these hydroxyl groups can oxidize the cobalt metal crystallites. Also, very recently Weng *et al.* (49) proposed that in the catalyst Rh/Al_2O_3 during the partial oxidation of methane, adsorbed water or OH groups on the alumina support can act as an oxygen source for oxidation reactions taking place on the Rh surface. It is envisaged here that the presence of hydroxyl groups on the Ln_2O_3 support could favor the reoxidation of cobalt during the reaction which deactivates, the catalyst and leads finally to regeneration of the perovskite structure. During the reduction and the reaction the H_2O present creates hydroxyl groups on the surface of the rare earth oxide according to the reaction

$$Ln_2O_3 + H_2O \rightleftarrows 2\,LnO(OH). \quad [9]$$

This reaction is more favorable for the La_2O_3 (as suggested by the CO TPD experiments; Figs. 5A–5C), which is probably due to its stronger basic character. It is possible that in the reaction conditions these hydroxyl groups, by reverse spillover, can reach the cobalt metal crystallites in the surface and in the bulk of the catalyst promoting its reoxidation. However, more detailed study is necessary to investigate this point. Another effect which could be present has been reported for the system M/Ln_2O_3/support (M = Rh and Pd; and Ln = La, Ce, Pr, Nd, and Sm) (31–33), where metal particles covered with partially reduced rare earth oxide "islands" show drastic changes in their surface and catalytic properties.

5. CONCLUSION

This work suggests that the high activity and selectivity of the catalysts Gd–Co–O and Sm–Co–O for the partial oxidation of methane to synthesis gas is due to the stability of the cobalt in its reduced state over the sesquioxides Gd_2O_3 and Sm_2O_3. In the case of La–Co–O and Nd–Co–O reoxidation of cobalt to the original perovskite structure causes loss of activity and selectivity. Reoxidation of the catalysts seems to be related to the thermodynamic stability of the parent perovskite structure. It is also suggested that the presence of hydroxyl groups on the rare earth oxide, especially in the La–Co–O system, might make some contribution to the reoxidation of cobalt metal via a reverse spillover phenomenon.

ACKNOWLEDGMENTS

This work was supported by Comision Interministerial de Ciencia y Tecnologia, Spain (Contract MAT95-0894). One of the authors (RML) is grateful to the Ministerio de Educacion y Ciencia, Spain, for the award of a postdoctoral fellowship. The authors acknowledge Mr. E. Pardo for his assistance in recording the photoelectron spectra.

REFERENCES

1. Tindall, B. M., and Crews, M. A., *Hydroc. Proc.* **11**, 75 (1995).
2. Tsang, S. T., Claridge, J. B., and Green, M. L. H., *Catal. Today* **23**, 3 (1995).
3. Ashcroft, A. T., Cheetham, A. K., Food, J. S., Vernon, P. D. F., and Green, M. L. H., *Nature* **344**, 319 (1990).
4. Hickman, D. A., and Schmidt, L. D., *Science* **259**, 343 (1993).
5. Dissanayake, D., Rosynek, M. P., and Lunsford, J. H., *J. Phys. Chem.* **97**, 3644 (1993).
6. Dissanayake, D., Rosynek, M. P., Kharas, K. C. C., and Lunsford, J. H., *J. Catal.* **132**, 117 (1991).
7. Peña, M. A., Gomez, J. P., and Fierro, J. L. G., *Appl. Catal.* **144**, 7 (1996).
8. Hayakawa, T., Andersen, A. G., Shimizu, M., Suzuki, K., and Takehira, K., *Catal. Lett.* **22**, 307 (1993).

9. Slagten, A., and Olbsbye, U., *Appl. Catal.* **110**, 99 (1994).
10. Choudhary, V. R., Rajput, A. M., and Rane, V. H., *Catal. Lett.* **16**, 269 (1992).
11. Hu, Y. H., and Ruckenstein, E., *J. Catal.* **158**, 260 (1996).
12. Hu, Y. H., and Ruckenstein, E., *Catal. Lett.* **35**, 265 (1995).
13. Choudhary, V. R., Uphade, B. S., and Mamman, A. S., *Catal. Lett.* **32**, 387 (1995).
14. Chu, Y., Li, S., Lin, J., Gu, J., and Yang, Y., *Appl. Catal. A General* **134**, 67 (1996).
15. Borowiecki, T., *Appl. Catal.* **10**, 273 (1984).
16. Rostrup-Nielsen, J. R., *in* "Catalysis Science and Technology" (J. R. Anderson and M. Boudart, Eds.), Vol. 5, p. 1. Springer, Berlin, 1984.
17. Rostrup-Nielsen, J. R., "Steam Reforming Catalysts." Teknisk Forlag A/S, Copenhagen, 1975.
18. Ruckenstein, E., and Hu, Y. H., *Appl. Catal. A General* **133**, 149 (1995).
19. Theron, J. N., Fletcher, J. C. Q., and O'Connor, C. T., *Catal. Today* **21**, 489 (1994).
20. Hayakawa, T., Andersen, A. G., Shimizu, M., Suzuki, K., and Takehira, K., *Catal. Today* **24**, 237 (1995).
21. Tascon, J. M. D., Mendioroz, S., and Tejuca, L. G., *Z. Phys. Chem. NF* **124**, 109 (1981).
22. Reuel, R. C., and Bartholomew, C. H., *J. Catal.* **85**, 63 (1984).
23. Crespin, M., and Hall, W. K., *J. Catal.* **69**, 359 (1981).
24. Chuang, T. J., Brundle, C. R., and Rice, D. W., *Surf. Sci.* **60**, 286 (1976).
25. Marcos, J. M., Buitrago, R. H., and Lombardo, E. A. *J. Catal.* **105**, 95 (1987).
26. Somorjai, G. A., "Introduction to Surface Chemistry and Catalysis." Wiley Interscience, New York, 1994.
27. Choi, J. G., *Catal. Lett.* **35**, 291 (1995).
28. Cortes, J., and Droguett, S., *J. Catal.* **38**, 437 (1975).
29. Heal, M. H., Leisegang, E. C., and Torrington, R., *J. Catal.* **51**, 314 (1978).
30. Bridge, M. E., Conrie, C. M., and Lambert, R., *J. Catal.* **58**, 28 (1979).
31. Ansorge, J., and Forster, H., *J. Catal.* **68**, 182 (1981).
32. Rieck, J. S., and Bell, A. T., *J. Catal.* **99**, 278 (1986).
33. Underwood, R. P., and Bell, A. T., *J. Catal.* **109**, 61 (1988).
34. Borer, A. L., and Prins, R., *J. Catal.* **144**, 439 (1993).
35. Lacombe, S., Holmen, A., Wolf, E. E., Ducarme, V., Moral, P., and Mirodatos, C., *in* "Natural Gas Conversion II" (C. C. Hyde and R. F. Howe, Eds.), p. 211. Elsevier, Amsterdam, 1994.
36. Lacombe, S., Zanthoff, H., and Mirodatos, C., *J. Catal.* **155**, 106 (1995).
37. Bernal, S., Botana, F. J., Garcia, R., and Rodriguez, J. M., *Thermochim. Acta* **66**, 139 (1983).
38. Turcotte, R. P., Sawyer, J. O., and Eyring, L., *Inorg. Chem.* **8**, 238 (1969).
39. Bernal, S., Dias, J. A., Garcia, R., and Rodriguez, J. M., *J. Mater. Sci.* **20**, 537 (1985).
40. Squire, G. D., Luc, H., and Puxley, D. C., *Appl. Catal. A General* **108**, 261 (1994).
41. Jackson, S. D., *J. Chem. Soc. Faraday Trans. I* **81**, 2225 (1985).
42. Wells, A. F., *in* "Structural Inorganic Chemistry," 4th ed., p. 450. Oxford Univ. Press, Oxford, 1975.
43. Futai, N., Yonghua, C., and Louhui, L., *React. Kinet. Catal. Lett.* **31**, 47 (1986).
44. Fierro, J. L. G., Tascon, J. M. D., and Tejuca, L. G., *J. Catal.* **93**, 83 (1985).
45. Tascon, J. M. D., Olivan, A. M., Tejuca, L.G., and Bell, A. T., *J. Phys. Chem.* **90**, 791 (1986).
46. Fierro, J. L. G., Tascon, J. M. D., and Tejuca, L. G., *Adv. Catal.* **36**, 237 (1989).
47. Katsura, T., Kitayama, K., Sugihara, T., and Kimizura, M., *Bull. Chem. Soc. Jpn.* **48**, 1809 (1975).
48. Weng, D., Dewaele, O., Groot, A. M., and Froment, G. F., *J. Catal.* **159**, 418 (1996).